Water Resources Research

RESEARCH ARTICLE
10.1029/2019WR026577

Geologic Controls on Source Water Drive Baseflow Generation and Carbon Geochemistry: Evidence of Nonstationary Baseflow Sources Across Multiple Subwatersheds

C. M. Richardson[1], **M. A. Zimmer**[1], **J. K. Fackrell**[1], **and A. Paytan**[2]

[1]Earth and Planetary Sciences, University of California Santa Cruz, Santa Cruz, CA, USA, [2]Institute of Marine Sciences, University of California Santa Cruz, Santa Cruz, CA, USA

Key Points:
- Both deep and shallow subsurface flow paths contribute to baseflow during the summer dry down period
- Differences in contributions of shallow and deep subsurface flow paths to baseflow across subwatersheds are related to local geology
- Stream water dissolved carbon geochemistry fluctuates in line with shifting sources during the summer dry down period

Supporting Information:
- Supporting Information S1

Correspondence to:
C. M. Richardson,
cmrichar@ucsc.edu

Citation:
Richardson, C. M., Zimmer, M. A., Fackrell, J. K., & Paytan, A. (2020). Geologic controls on source water drive baseflow generation and carbon geochemistry: Evidence of nonstationary baseflow sources across multiple subwatersheds. *Water Resources Research*, *56*, e2019WR026577. https://doi.org/10.1029/2019WR026577

Received 21 OCT 2019
Accepted 18 MAY 2020
Accepted article online 26 MAY 2020

Abstract The contributions and composition of baseflow sources across an extended recession period were quantified for six subwatersheds of varying size in a structurally complex watershed in coastal California using endmember mixing analysis and related to catchment characteristics (e.g., topography, geology, land use, and soil characteristics). Both shallow subsurface and deep groundwater reservoirs were important contributors for streamflow during low flow periods, and the composition of baseflow sources across subwatersheds was directly related to geologic indices. A binary classification of underlying bedrock permeability (e.g., low vs. high) best explained the changes in shallow subsurface water and deeper groundwater inputs through the seasonal recession. Dissolved inorganic carbon (DIC), dissolved organic carbon (DOC), and specific UV absorbance at 254 nm ($SUVA_{254}$) were used to provide additional insight into endmember characteristics and their contributions to baseflow. Stream water DIC concentrations were broadly controlled by mixing of groundwater and shallow subsurface water endmembers with relatively constant DIC concentrations, while stream water DOC concentrations reflected both spatial and temporal changes in shallow subsurface water DOC. Results from this study show (1) the importance of considering baseflow as a dynamic mixture of water from multiple sources, (2) the effect of geology on source composition at the subwatershed scale during low flow conditions, and (3) the impact of shifting baseflow sources on stream water dissolved carbon concentrations and the utility of using dissolved carbon concentrations to obtain additional insight into temporal variability in baseflow sources.

1. Introduction

Structural characteristics of watersheds (e.g., area, slope, and bedrock type) have been used to aid in understanding and predicting streamflow generation in many systems (Jencso & McGlynn, 2011; McGuire et al., 2005; Price, 2011). Most work relating watershed characteristics to streamflow generation focuses on dynamic periods of the annual hydrograph (rainfall events or snowmelt periods), and knowledge gaps still exist regarding controls on baseflow. Baseflow is often characterized as a geochemically static component of streamflow that is sustained by regional groundwater (GW) (Klaus & McDonnell, 2013). This characterization of baseflow as temporally uniform and spatially homogenous may be inappropriate for many systems.

Previous work has documented significant spatial variability in stream geochemistry during low flow periods (Asano et al., 2009; Blumstock et al., 2015; Soulsby et al., 2007; Temnerud et al., 2010; Tetzlaff & Soulsby, 2008; Zimmer et al., 2013). Variability in stream geochemistry across stream networks during low flow periods is often indicative of multiple source waters, which typically have distinct endmember chemistry due to differences in routing and storage in the subsurface (Payn et al., 2012). Blumstock et al. (2015) found that stream water chemistry of a montane watershed became increasingly heterogeneous as baseflow progressed, suggesting GW contributions from multiple geochemically distinct hydrological units. Others also found that several GW or shallow flow path sources can contribute to streamflow during baseflow (Costelloe et al., 2015; Smerdon et al., 2012).

Variability in recession curve behavior (e.g., slope, timing, and length) between and within watersheds also highlight that multiple sources and flow paths contribute to baseflow (Tallaksen, 1995). Baseflow is commonly considered to be composed of delayed or slow flow path sources. These slow flow paths are not

limited to deep GW reservoirs and may include shallow subsurface reservoirs (Anderson & Burt, 1980; Hewlett & Hibbert, 1963; McCallum et al., 2010; Smakhtin, 2001). To account for variability in recession behavior, Stoelzle et al. (2019) developed a new baseflow separation index that considers dynamic contributions from multiple sources during recession periods. Taken together, these studies on stream water geochemical variability and recession behavior during low flow periods raise critical questions about (1) the importance of runoff contributions from slow flow paths other than deep GW and (2) how and why different water source contributions vary in time and space during baseflow.

Spatial variability in stream water sources within watersheds during baseflow may be predicted or explained by internal variability in catchment characteristics. Cohesive frameworks that integrate spatial predictors across space and time are needed (Sivapalan, 2003). In an effort to build on this need, a range of watershed characteristics, such as climate, topography, geology, soil, vegetation, and land use, have been linked to streamflow generation processes (Buttle et al., 2004; Carlier et al., 2018; Emanuel et al., 2010; Jencso & McGlynn, 2011; Onda et al., 2006). Work focused exclusively on baseflow generation processes also shows connections to geology (Bloomfield et al., 2009; Price, 2011; Tague & Grant, 2004). Variability in water sources and their relative contributions to baseflow may be especially important in structurally complex watersheds, where flow pathways can vary at the subwatershed scale. Heterogeneous watersheds provide a unique opportunity to examine and integrate the importance of suggested hierarchal controls (e.g., climate, geology, soil, and vegetation) on hydrologic processes beyond commonly considered topographic indices (Bergstrom et al., 2016; Devito et al., 2005; Zimmer & Gannon, 2018). For example, Payn et al. (2012) used structurally diverse subwatersheds to relate topographic and geologic characteristics to baseflow generation processes and found that during baseflow recession, the importance of structural controls increased while the importance of topographic controls decreased.

Identification of sources using a multitracer approach may be useful for defining and distinguishing among the dominant contributors to baseflow. Geochemical differences between potential slow flow sources can be used to separate their relative contributions to baseflow as is frequently done for higher flow periods (Klaus & McDonnell, 2013). Multitracer approaches can also be best leveraged in structurally complex watersheds where differences in source contributions may be largest.

In this study, we examine the spatial distribution and temporal evolution of baseflow sources in a structurally complex central coastal California watershed and their relationship to spatial controls (e.g., topography, geology, land use, and soil characteristics) based on four synoptic sampling events during the summer dry down season lasting ~6 months. We leverage the extended recession period typical of Mediterranean climate catchments to isolate the nature of contributions to baseflow in the absence of complicating rainfall events typical of many other systems. To do this, we used endmember mixing analysis (EMMA) to examine how source water contributions shift across the seasonal baseflow recession period in six geologically diverse subwatersheds. We relate the EMMA results to spatial characteristics of the subwatersheds to better understand hierarchal controls on source contributions to flow. Specifically, we aim to answer the following questions:

1. What water sources sustain baseflow at the subwatershed scale, and do their proportions change with time and in space?
2. Are baseflow sources and magnitudes correlated to subwatershed spatial characteristics?
3. How do baseflow sources relate to variability in stream geochemistry, specifically dissolved carbon concentrations?

2. Materials and Methods

2.1. Study Area

The San Lorenzo River (SLR) drains the 360 km^2 San Lorenzo Watershed (SLW) in central coastal California (Figure 1a). Discharge in the SLR is generally controlled by seasonal precipitation, which is characterized by winter maxima and summer minima typical of Mediterranean climates. This wet-dry seasonality often results in extended recession periods that start in late spring and persist through early fall. Average annual precipitation in the SLW was ~1,090 $\pm$ 527 mm for Water Years (WY) 2011 to 2018, as measured at Station US1CASZ0024 in Felton, California (accessed via NOAA National Centers for Environmental Information

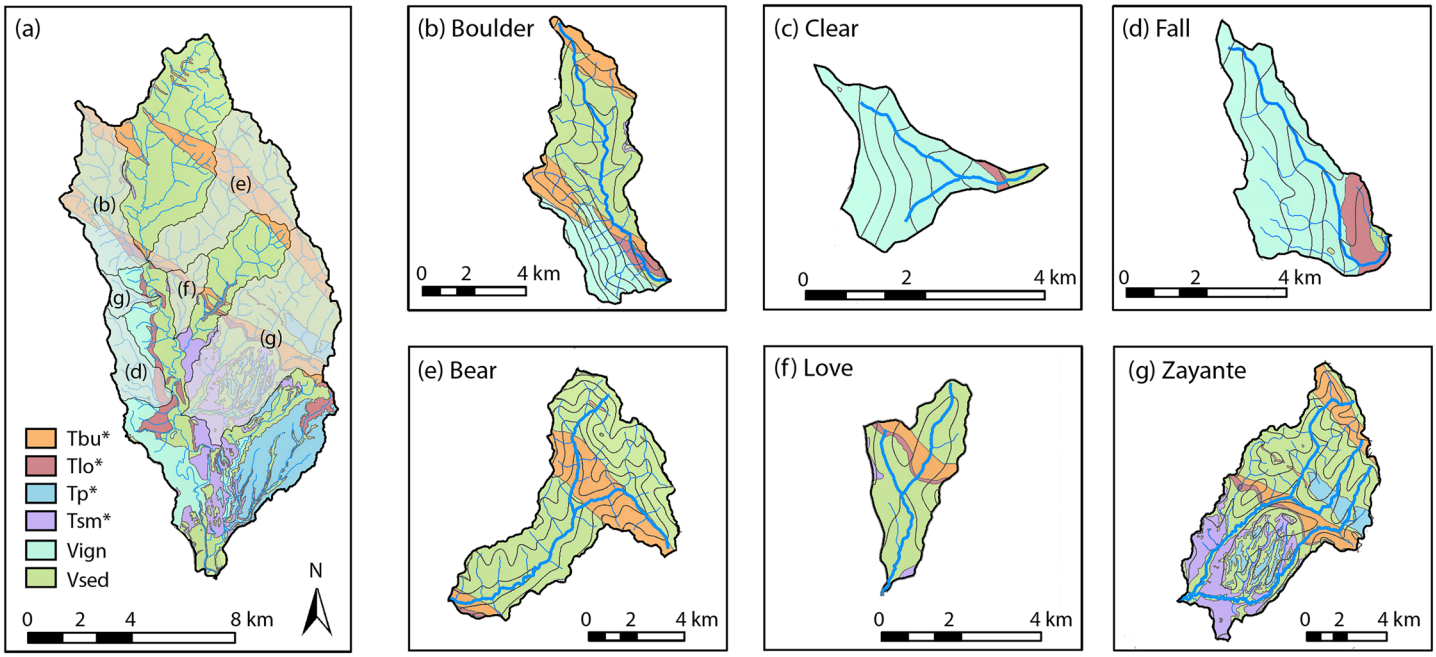

Figure 1. (a) Geologic map of the San Lorenzo Watershed in Santa Cruz County, California. Asterisks indicate water-bearing units. Tbu, Tertiary Butano sandstone; Tlo, Tertiary Lompico sandstone; Tp, Tertiary Purisima Formation; Tsm, Tertiary Santa Margarita sandstone; Vign, various nonwater-bearing igneous and metamorphic facies; Vsed, various nonwater-bearing sedimentary units. Gray-shadowed regions depict the studied subwatersheds. (b–g) Geologic maps of the subwatersheds. Contour lines represent 100 m changes in elevation.

Climate Data Online) (NCDC, 2019). The sampling period herein consists of the summer of WY 2018 (October 2017 to September 2018), a year with below average precipitation (692 mm).

The SLW consists of more than 20 subwatersheds, each draining primary tributaries that directly discharge into the mainstem SLR. This study focused on six subwatersheds in the SLW that vary in size from 3.7 to 69.5 km^2 (Figures 1b–1g). Boulder, Clear, and Fall creeks originate from western subwatersheds, while Bear, Love, and Zayante creeks drain eastern subwatersheds.

The watershed has complex lithology (Figure 1). Regional GW inputs to surface waters arise from three potential water-bearing units: Butano sandstone, Lompico sandstone, and Santa Margarita sandstone (ETIC Engineering, 2006). The Santa Margarita sandstone is a high permeability, generally unconfined unit with exposures along Boulder, Love, and Zayante creeks. The Butano sandstone has surface exposures in areas along Bear, Boulder, Love, and Zayante creeks but generally underlies the Lompico sandstone, which has surface exposures in all subwatersheds. Western subwatersheds of the SLW have high-grade metamorphic (e.g., schist) and igneous (e.g., granodiorite) bedrock, while eastern subwatersheds are underlain by primarily sedimentary bedrock. Soil parent material for the SLW is weathered sandstone and occasionally weathered granite; soils are generally well drained sandy loam mollisols. Vegetation in the SLW is dominated by evergreens, including native coastal redwoods (*Sequoia sempervirens*) and Douglas fir (*Pseudotsuga menziesii*).

2.2. Spatial Analysis of Subwatershed Characteristics

Geologic, topographic, land use, and soil characteristics were aggregated for each subwatershed in ArcGIS. Land cover was based on the 30 m spatial resolution National Land Cover Database (NLCD) from 2011 (NLCD, 2011). Open space percentage includes the following NLCD classifications: "Developed, Open Space," "Shrub," "Grassland," and "Pasture." Forest percentages used in this study are the sum of "Evergreen Forest" and "Mixed Forest." Classification definitions are available online from the NLCD database. Soil characteristics were extracted from the National Soil Conservation Service Soil Survey Geographic (SSURGO) database using the Web Soil Survey tool (SSURGO, 2019). Topographic data were aggregated from a patched USGS 3 m DEM from Fisher et al. (2016). Bedrock cover was

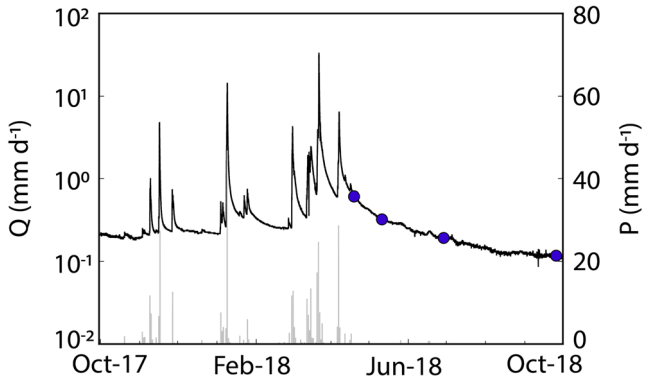

Figure 2. San Lorenzo River mainstem specific discharge (Q) at USGS 11160500 and daily precipitation (P) for the 2018 water year at NCDC Station US1CASZ0024. Synoptic sampling events are indicated by blue markers on the hydrograph.

analyzed using a digital geological map of Santa Cruz County based on Brabb et al. (1997). Bedrock permeability was classified in a binary manner by setting a threshold hydraulic conductivity value of 10^{-9} m s^{-1} (e.g., an intrinsic permeability of ~10^{-16} m^2), with values below this threshold considered low permeability. Aquifer test results compiled by Kennedy/Jenks (2015) were used to classify water-bearing units. Nonwater-bearing units (e.g., granite, shale, and schist) were assumed to have hydraulic conductivity values of 10^{-10} to 10^{-13} m s^{-1}, based on values given from Freeze and Cherry (1979).

2.3. Water Sampling and Stream Gauging

Water samples were collected from six streams (Bear, Boulder, Clear, Fall, Love, and Zayante) during four single-day sampling events in April, May, June, and September of 2018, as mainstem discharge receded in the absence of major precipitation events (Figure 2). Nearly 98% of rainfall in WY 2018 occurred between October and early April, prior to the sampling events. GW samples were collected from eight established monitoring wells in the watershed during a separate sampling event in June 2018. All water samples were filtered to 0.2 μm and refrigerated immediately after sampling until geochemical analysis at the Marine Analytical Lab at the University of California at Santa Cruz (UCSC). Cation concentrations (Na^+, Ca^{2+}, Mg^{2+}, and K^+) were measured using a Thermo iCAP 7400 Inductively Coupled Plasma Optical Emission Spectrometer. Anion concentrations (Cl^- and SO_4^{2-}) were measured on a Dionex ICS-2000 Ion Chromatograph. Major dissolved inorganic nutrients (NO_3^-, PO_4^{3-}, and SiO_4^{4-}) were determined on a Lachat QuikChem 8000 Flow Injection Analyzer. Dissolved organic carbon (DOC) was measured as nonpurgeable organic carbon (NPOC) on a Shimadzu TOC-VCPH TC/TN Analyzer, and dissolved inorganic carbon (DIC) was determined on a UIC Carbon Coulometer. Specific ultraviolet absorbance ($SUVA_{254}$) at 254 nm, a measure of percent aromaticity considered to represent DOC reactivity, was measured on a Thermo Genesys 10S UV-Visible Spectrophotometer (Weishaar et al., 2003). Analytical precision and accuracy for all analytes was generally better than 5% (supporting information Table S1).

At the time of water sample collection, each stream was gauged just upstream of its confluence with the mainstem of the SLR using a Pygmy Price flow meter at 0.6 of the water depth. Flow was calculated using the velocity-area method according to Rantz (1982). Stream velocity was generally measured at intervals such that no more than 10% of streamflow was contained in one subsection (6.9 ± 2.3% in April, 6.0 ± 1.2% in May, 6.1 ± 1.7% in June, and 8.2 ± 1.8% in September 2018).

2.4. Baseflow Separation Using Endmember Mixing Analysis

Endmember mixing analysis (EMMA) was used to divide inputs to streams into either GW or shallow subsurface water (SSW) (Christophersen et al., 1990; Christophersen & Hooper, 1992; Hooper et al., 1990). Ten tracers (Na^+, Ca^{2+}, Mg^{2+}, K^+, Cl^-, SO_4^{2-}, NO_3^-, PO_4^{3-}, SiO_4^{4-}, and specific conductivity) were considered for use and evaluated for conservative behavior. Tracers were defined as conservative if they exhibited at least one linear trend in bivariate solute-solute plots (R^2>0.5, p <0.01) (Figure S1). The final selected model indicated three endmembers and used eight tracers (Na^+, Ca^{2+}, Mg^{2+}, Cl^-, SO_4^{2-}, NO_3^-, PO_4^{3-}, and specific conductivity). The model conformed to requirements of low residual structure (mean R^2 = 0.07 ± 0.05) and high cumulative variance in accordance with the "rule of 1" (m = 2, PC1 = 73.9%, PC2 = 18.3%) (Table S2) (Hooper, 2003).

Since multiple water-bearing units have the potential to contribute to baseflow in the SLW, we used results of the spatial analysis of subwatershed lithology combined with previous work indicating plausible GW contributions to the studied streams to inform all possible GW endmembers for each stream in EMMA (Table S3) (ETIC Engineering, 2006). The geochemistry of each GW endmember was based on the average concentrations of the collected water samples and corroborated with historical records (Table S4). NO_3^- and PO_4^{3-} concentrations used in EMMA were particularly useful for fingerprinting GW contributions from anthropogenically impacted aquifers in the region (e.g., Santa Margarita and Lompico). All GW contributions herein are presented as the sum of GW fractions determined via EMMA.

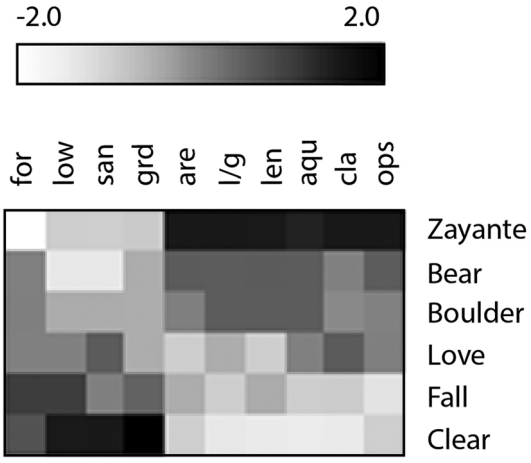

Figure 3. Heatmap visualization of subwatershed characteristics. Characteristics were centered by the mean and scaled by the standard deviation. aqu, %aquifer; are, watershed area; cla, %clay in soil; for, %forest; grd, mean stream gradient; l/g, stream length/mean gradient; len, stream length; low, %low-permeability bedrock; ops, %open space; san, %sand in soil. See Table S5 for the actual values.

Many studies exist showing large variability in soil water chemistry over relatively small scales in forested catchments (Grossmann & Kloss, 1994; Manderscheid & Matzner, 1995). Instead of direct sampling, which would be difficult to accomplish over the spatial scale of this study, we assumed a range in viable SSW endmember geochemistry based on a thorough examination of mixing dynamics across flow conditions in the SLR using historical and current water-quality data from the California Environmental Protection Agency's Central Coastal Ambient Monitoring Program (CCAMP, 2019). Principal component analysis (PCA) of available water-quality data (Cl^-, Na^+, PO_4^{3-}, NO_3^-, and specific conductivity) was completed using mainstem SLR data for three water years for which both discharge and geochemical data were available (WY 2005, 2011, and 2017) at USGS 11160500. The PCA revealed two distinct data clusters that separated out as a function of flow conditions: low- to intermediate-discharge periods and intermediate- to high-discharge periods (Figure S2). These clusters, which shed light on how water sources to the SLR operate seasonally, regardless of antecedent conditions, were confirmed with *k*-means cluster analysis (Figure S2). At low flows, PCA results indicated a transition in dominant source contributions, likely representing diminished inputs from SSW and increases in GW contributions. Given knowledge of GW endmember geochemistry for the region, the SSW source must be a low conductivity, low ionic strength endmember that more closely resembles geochemistry observed during mid- to high-discharge periods. As such, the stream with the lowest conductivity and cation/anion concentrations during the first sampling event in March 2018 was used as the upper boundary of SSW geochemistry. To complement this upper boundary geochemistry estimate, we assumed the lowest concentration SSW endmember was close to regional rainwater chemistry (e.g., equivalent to the shortest possible residence time with no significant interaction with subsurface strata). We used a 5 year average (2013–2017) rainwater geochemical profile from National Trends Network (Site CA 66), which is part of the National Atmospheric Deposition Program (NTN, 2019) to estimate the lowest concentration SSW endmember.

These endmember estimates assume that SSW geochemistry, with respect to the parameters used in EMMA, is relatively uniform across the watershed, an assumption we believe to be reliable for the needs of this study based on (1) spatial analyses of soil characteristics that show general homogeneity in soil types across the watershed examined, (2) supporting DIC data independent of the EMMA model as presented in section 4, and (3) expectations that intrasource geochemical variability of the SSW endmember is likely low with respect to across source variability (relative to GW endmembers) from large differences in residence times. We recognize that the fractions generated in EMMA are biased by our endmember approximation but believe that the resulting estimate is sufficient for the goals of this paper as both SSW endmembers represent geochemical extremes, but even at their upper and lower boundaries, the resulting shifts in contributions from the SSW endmember, as determined via EMMA, were generally small (5.6 ± 4.5%, see Figure 5).

2.5. Correlation Analysis

Cross correlations of spatial characteristics were analyzed using Pearson's correlation coefficient (R) after confirming that the distributions were not significantly different from normal using a Kolmogorov-Smirnov normality test. Relationships between spatial characteristics and derived quantities from streamflow and source fractions were analyzed using the nonparametric Spearman's rank correlation coefficient (r_s). Average values are denoted herein as "$\bar{x}$" and typically presented with their 1-sigma standard deviation.

3. Results

3.1. Analysis of Subwatershed Spatial Characteristics

There was a clear gradient in spatial characteristics across the subwatersheds (Figure 3 and Table S5), and the majority of the considered characteristics were correlated (Figure S3). For example, smaller

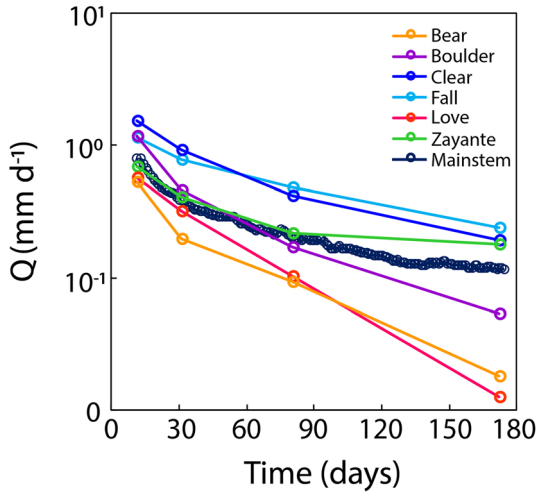

Figure 4. Time (days) versus specific discharge, Q (mm day^{-1}), for all streams. Mainstem Q is shown for USGS 11160500. Markers represent the sampling events.

subwatersheds were generally steeper with shorter flow paths and greater spatial extents of low-permeability bedrock compared to larger subwatersheds. Larger subwatersheds also had greater fractions of their area underlain by aquifers ($R^2 = 0.87$, $p<0.05$). Land use cover across the subwatersheds was relatively uniform with forests covering 75% to 88% of the subwatersheds, though these slight differences were strongly negatively correlated with other characteristics such as open space cover, subwatershed area, length/gradient, aquifer area, and soil sand/clay content (Figure S3). The secondary dominant land cover for all subwatersheds was open space, which ranged from 10% to 20%. Physical characteristics of soils were also relatively uniform in terms of sand content (61 ± 3%) and clay content (17 ± 2%). Soil organic matter (SOM) content varied slightly across the study area, with eastern subwatersheds containing slightly higher SOM (2.2 ± 0.2%) relative to western subwatersheds (1.3 ± 0.2%; Table S6).

3.2. Baseflow Magnitude and Endmember Contributions to Streamflow

Discharge normalized by watershed area, defined as specific discharge (Q), decreased in all streams across the study period (Figure 4). Specific discharge from all streams averaged 0.94 ± 0.41 mm day^{-1} in April, 0.51 ± 0.28 mm day^{-1} in May, 0.25 ± 0.17 mm day^{-1} in June, and 0.12 ± 0.10 mm day^{-1} in September of 2018. Between April and September of 2018, specific discharge decreased on average by 0.83 ± 0.36 mm day^{-1}, or 88 ± 10%, in all streams. Western streams (Boulder, Clear, and Fall) had higher specific discharges initially relative to eastern streams (Bear, Love, and Zayante; 1.15 to 1.54 vs. 0.53 to 0.69 mm day^{-1}, respectively). Of the three western streams with high initial specific discharge, Fall and Clear creeks maintained the highest specific discharges through the entire recession period, and initial spatial differences observed in specific discharge across most streams were similar through the dry down period.

The fraction of SSW (f_{SSW}) generally decreased through time in all streams, though not all transitioned to GW dominance, which we define here as an f_{GW} greater than 0.5 (Figure 5). In April 2018, four (Boulder, Clear, Fall, and Love) of the six streams were SSW dominated (defined as f_{SSW} greater than 0.5). Of the four initial SSW-dominated streams, only Boulder Creek transitioned to GW dominance by September 2018. f_{SSW} decreased on average by 0.15 ± 0.07 in all streams across the recession period. The largest and smallest decreases in f_{SSW} occurred in Boulder Creek (−0.26) and Zayante Creek (−0.08), respectively (Figure 5).

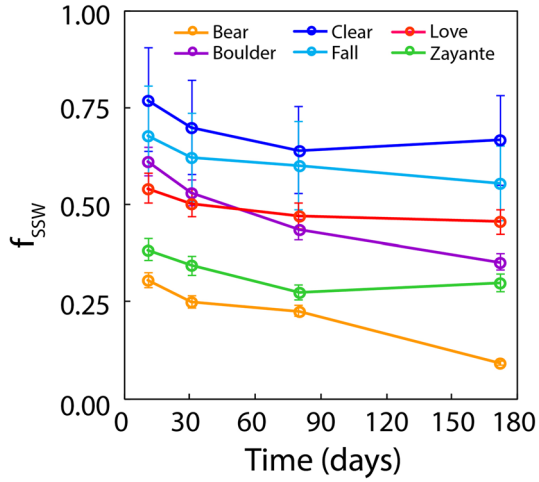

Figure 5. Time (days) versus fraction of stream water baseflow from SSW (f_{SSW}) for all streams. Error bars represent the range of fractions produced using the upper and lower estimates of SSW endmember geochemistry. Markers represent the sampling events.

Specific discharge from SSW (Q_{SSW}) ranged from 0.16 to 1.19 mm day^{-1} in April ($\bar{x}$ = 0.57 ± 0.39 mm day^{-1}), 0.05 to 0.64 mm day^{-1} in May ($\bar{x}$ = 0.29 ± 0.23 mm day^{-1}), 0.02 to 0.29 mm day^{-1} in June ($\bar{x}$ = 0.13 ± 0.12 mm day^{-1}), and 0.002 to 0.13 mm day^{-1} in September of 2018 ($\bar{x}$ = 0.06 ± 0.06 mm day^{-1}) (Figure 6a). Q_{SSW} decreased on average by 91 ± 8% in all streams during the summer dry down period, and the largest decreases in Q_{SSW} generally occurred in western streams (Boulder, Clear, and Fall). Q_{GW} ranged from 0.26 to 0.46 mm day^{-1} in April ($\bar{x}$ = 0.38 ± 0.07 mm day^{-1}), 0.15 to 0.30 mm day^{-1} in May ($\bar{x}$ = 0.23 ± 0.06 mm day^{-1}), 0.07 to 0.20 mm day^{-1} in June ($\bar{x}$ = 0.12 ± 0.05 mm day^{-1}), and 0.007 to 0.11 mm day^{-1} in September of 2018 ($\bar{x}$ = 0.06 ± 0.05 mm day^{-1}) (Figure 6b). Q_{GW} decreased on average by 85 ± 12% in all streams during the study period.

3.3. Relationship of Baseflow Magnitude and Source to Subwatershed Characteristics

The relationship between specific discharge, f_{SSW}, Q_{SSW}, and Q_{GW} was examined with respect to subwatershed characteristics to evaluate

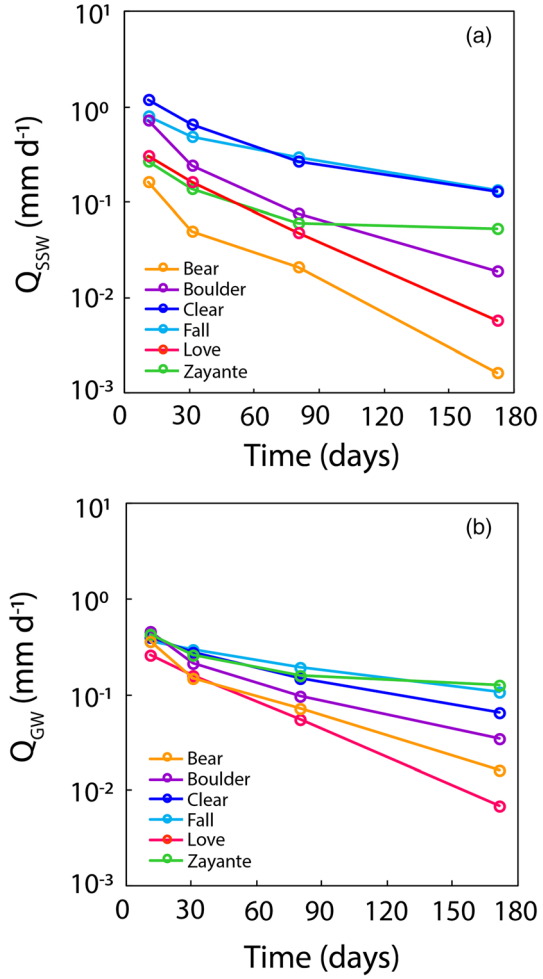

Figure 6. Time (days) versus (a) specific discharge (mm day^{-1}) from SSW (Q_{SSW}) and (b) specific discharge from GW (Q_{GW}) for all streams. Markers represent the sampling events.

potential first-order spatial predictors (Table 1). Specific discharge was not correlated to any of the spatial predictors considered in this study. The binary index of bedrock permeability was the best stand-alone predictor of f_{SSW} (r_s = 0.94 to 1.00, p<0.05) (Figure 7). Q_{SSW} was best predicted by the fraction of the catchment with low-permeability bedrock initially (r_s = 0.94, p<0.05), though this correlation's significance decreased through the recession period. There were no statistically significant correlations for Q_{GW}.

3.4. Stream Water Dissolved Carbon Geochemistry

Stream water DIC, DOC, and $SUVA_{254}$ values generally followed similar trends with time, though absolute changes in concentrations among the streams varied in magnitude (Figure 8). Across all subwatersheds, stream water DIC concentrations and $SUVA_{254}$ values generally increased, and stream water DOC concentrations decreased as f_{GW} increased through the recession period. Stream water DIC concentrations and $SUVA_{254}$ values increased on average by 450 ± 300 μM and 1.8 ± 0.3 L mg^{-1} m^{-1}, respectively, while stream water DOC concentrations decreased on average by 120 ± 50 μM through the dry season.

Spatial differences in stream water DOC concentrations and $SUVA_{254}$ values across subwatersheds were also apparent. Stream water DOC concentrations ranged from 130 to 390 μM ($\bar{x}$ = 250 ± 100 μM) at the start of the dry season (April 2018) and decreased to 60 to 200 μM ($\bar{x}$ = 130 ± 70 μM) by the end of the study period (September 2018) (Figure 8b). $SUVA_{254}$ values in stream water were spatially variable as well and ranged as follows: 1.2 to 2.3 L mg^{-1} m^{-1} in April ($\bar{x}$ = 1.9 ± 0.5 L mg^{-1} m^{-1}), 2.3 to 3.2 L mg^{-1} m^{-1} in May ($\bar{x}$ = 2.6 ± 0.3 L mg^{-1} m^{-1}), 2.1 to 3.7 L mg^{-1} m^{-1} in June ($\bar{x}$ = 3.1 ± 0.6 L mg^{-1} m^{-1}), and 3.4 to 4.1 L mg^{-1} m^{-1} in September of 2018 ($\bar{x}$ = 3.6 ± 0.3 L mg^{-1} m^{-1}) (Figure 8c).

4. Discussion

4.1. Geologic Controls on Nonstationarity in Baseflow Sources

Many studies on streamflow generation mechanisms have focused exclusively on topographic indices as spatial predictors. This approach is well suited for structurally homogeneous systems where geology is generally uniform (McGuire et al., 2005). In more structurally complex landscapes, geologic controls may override topographic predictors of streamflow generation processes. Subwatersheds of the SLW were primarily distinguished by differences in bedrock permeability. By leveraging these spatial differences in geology during the summer dry down period, we were able to show that the relative contribution of SSW and deep GW to streamflow was best explained by subwatershed-scale differences in bedrock permeability (Table 1). This finding is in line with previous work that has suggested that bedrock permeability is an important control on subsurface flow pathways and transit times (Pfister et al., 2017; Uchida et al., 2006), especially during baseflow (Hale et al., 2016; Hale & McDonnell, 2016; Jencso & McGlynn, 2011; Tague & Grant, 2004). These spatial differences in bedrock permeability translated to physical distinctions in available subsurface water storage capacity (Figure 9). In subwatersheds with greater areal extents of high-permeability bedrock, relative contributions of GW to streamflow were the highest. High-permeability bedrock allows for vertical movement of water, via infiltration and deeper recharge of GW reservoirs, which limits the extent of water accumulation in shallow subsurface storage and, subsequently, downslope SSW contributions to baseflow (Figures 9c and 9d). In contrast, subwatersheds with low-permeability bedrock transmitted water primarily through shallow subsurface pathways (Figure 9a). Streams in these subwatersheds received up to an order of magnitude more SSW than their more permeable counterparts and remained compositionally dominated by SSW through the entire recession period considered, even as specific discharge decreased across all streams

Table 1
Spearman's Rank Correlation Coefficients (r_s) Between Subwatershed Characteristics and Specific Discharge (Q), Fraction of Streamflow From Shallow Subsurface Water (f_{SSW}), Specific Discharge From SSW (Q_{SSW}), and Specific Discharge From GW (Q_{GW})

	Geology		Topography				Land use		Soil	
	% Aquifer	% Low Permeability	Area	Length	Gradient	L/G	% Forest	% Open Space	% Clay	% Sand
Q										
Apr 2018	−0.49	0.71	−0.49	−0.49	0.31	−0.37	0.64	−0.66	−0.71	0.60
May 2018	−0.64	0.83	−0.54	−0.54	0.49	−0.54	0.75	−0.77	−0.77	0.66
Jun 2018	−0.49	0.71	−0.31	−0.31	0.37	−0.43	0.64	−0.66	−0.54	0.49
Sep 2018	−0.49	0.71	−0.31	−0.31	0.37	−0.43	0.64	−0.66	−0.54	0.49
Cumulative	−0.14	0.07	−0.04	−0.04	0.26	−0.17	0.10	−0.06	−0.21	0.01
f_{SSW}										
Apr 2018	−0.81	0.94*	−0.77	−0.77	0.60	−0.71	0.84*	−0.89*	−0.83	0.83
May 2018	−0.81	0.94*	−0.77	−0.77	0.60	−0.71	0.84*	−0.89*	−0.83	0.83
Jun 2018	−0.90*	1.00**	−0.89*	−0.89*	0.66	−0.83	0.75	−0.83	−0.71	0.94*
Sep 2018	−0.90*	1.00**	−0.89*	−0.89*	0.66	−0.83	0.75	−0.83	−0.71	0.94*
Cumulative	−0.83	0.93	−0.80	−0.80	0.61	−0.75	0.77	−0.83	−0.74	0.85
Q_{SSW}										
Apr 2018	−0.81	0.94*	−0.77	−0.77	0.60	−0.71	0.84*	−0.89*	−0.83	0.83
May 2018	−0.81	0.94*	−0.77	−0.77	0.60	−0.71	0.84*	−0.89*	−0.83	0.83
Jun 2018	−0.58	0.77	−0.43	−0.43	0.43	−0.49	0.81	−0.83	−0.71	0.54
Sep 2018	−0.58	0.77	−0.43	−0.43	0.43	−0.49	0.81	−0.83	−0.71	0.54
Cumulative	−0.45	0.55	−0.37	−0.37	0.35	−0.40	0.50	−0.52	−0.47	0.43
Q_{GW}										
Apr 2018	0.40	−0.15	0.38	0.38	−0.41	0.49	−0.04	0.09	−0.09	−0.23
May 2018	−0.49	0.71	−0.31	−0.31	0.37	−0.43	0.64	−0.66	−0.54	0.49
Jun 2018	−0.12	0.31	0.14	0.14	0.14	−0.09	0.41	−0.37	−0.31	0.03
Sep 2018	−0.12	0.31	0.14	0.14	0.14	−0.09	0.41	−0.37	−0.31	0.03
Cumulative	−0.02	0.12	0.06	0.06	0.02	−0.01	0.12	−0.11	−0.12	0.02

*Significance of $p<0.05$. **Significance of $p<0.01$.

(Figure S4). Hale and McDonnell (2016) found similar differences in subsurface flow paths in catchments with contrasting underlying geology; in areas with low-permeability volcanic rock, storage was limited to shallow soils, and mean transit times in these areas were short (~1.8 years) relative to more sedimentary catchments with deeper GW reservoirs (~6.2 years). Such permeability contrasts at soil-bedrock contacts are known to initiate shallow downslope subsurface flow (Harr, 1977), and early studies on recession flows show that these shallow flowpaths can be active, long-duration contributors to streamflow in the absence of rainfall (Hewlett & Hibbert, 1963; Mosley, 1979). Additionally, while no work exists showing the extent of bedrock fracturing in the studied subwatersheds, it is possible that the shallow subsurface stores are influenced by exfiltration of bedrock GW into overlying soil layers (Figure 9b); catchments with significant fracturing of bedrock can receive 50% to 95% of baseflow contributions from bedrock GW (Uchida et al., 2003). The exact routing of water, from initial infiltration to final discharge from shallow subsurface storage, through the low-permeability subwatersheds is unclear without more detailed field-based work on flow paths.

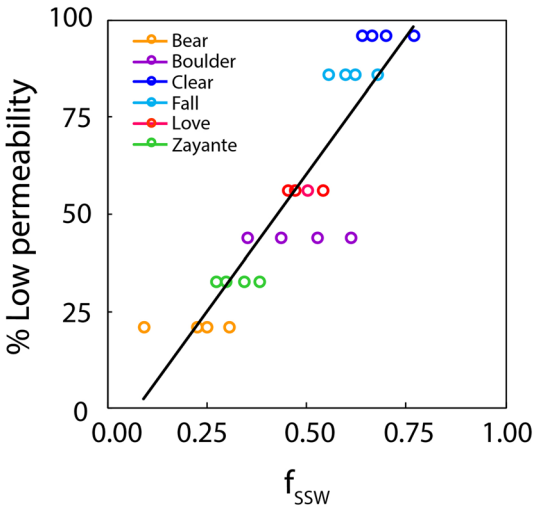

Figure 7. Fraction of stream water baseflow from SSW (f_{SSW}) versus percent of subwatershed with low-permeability bedrock. Markers represent the sampling events (r_s = 0.93, see Table 1).

Interestingly, the subwatersheds with the greatest areal extent of low-permeability bedrock were generally able to maintain the highest specific discharges through the recession period (from sustained SSW contributions) even though their specific discharges decreased the most in absolute terms. The drainage characteristics of SSW-dominated streams imply that subwatersheds with greater percentages of low-permeability bedrock can accumulate more water per area for initial rapid release from dynamic storage in the soil mantle and that this compartment drains

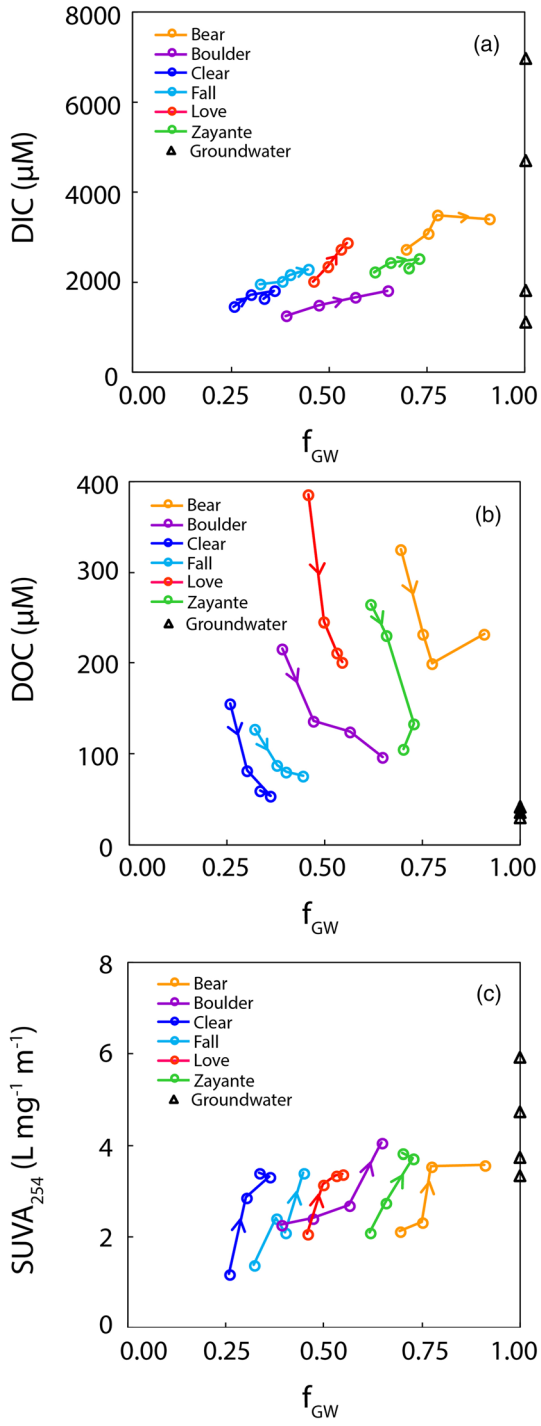

Figure 8. Fraction of stream water baseflow from GW (f_{GW}) versus (a) DIC concentration, (b) DOC concentration, and (c) $SUVA_{254}$. Markers represent the sampling events with time progressing in the direction of the arrow. Black triangles represent the range in GW endmember concentrations or values.

faster but less efficiently than deep GW stores. This inefficiency ties back to early experimental work by Hewlett and Hibbert (1963), which shows sustained soil mantle drainage can last over 140 days in the absence of rainfall. The finding of SSW-dominated streams is especially important in the context of emerging hydroclimatic variability. SSW-dominated streams may be more sensitive to seasonal and annual changes in precipitation as these stores depend on relatively recent precipitation (within the water year) for recharge, while primary aquifers are often better buffered against interannual precipitation variability (Nippgen et al., 2016; Zimmer & Gannon, 2018).

Similar to past work on scaling properties of structurally diverse catchments (Carlier et al., 2018; Hale et al., 2016; Hale & McDonnell, 2016; Tague & Grant, 2004), our finding of the importance of bedrock permeability in baseflow source partitioning emphasizes the value of including geologic indices in development of a hydrologic classification system (McDonnell & Woods, 2004; Wagener et al., 2007). Systems with strong correlations of topographic indices to properties of catchment function may actually represent finer-scale controls on water cycling and fit into studies such as this one, which leverages structural heterogeneity to delineate the higher spatial order control of geology. Such intercomparisons hint at the importance of geologic controls on catchment storage and release functions during low flow periods in geologically diverse, mountainous watersheds.

4.2. Implications of Shifting Baseflow Sources: An Example Using Dissolved Carbon Geochemistry

Spatial and temporal differences in water sources contributing to baseflow have consequences for observed stream biogeochemistry. Variability in concentrations of biologically relevant compounds, such as dissolved carbon, across and within structurally complex watersheds during baseflow may arise primarily from differences in water sources rather than in-stream biogeochemical processing. We found that dissolved carbon concentrations and associated $SUVA_{254}$ values shifted in line with changes in dominant source contributions (Figure 8). Though the exact concentrations of dissolved carbon in streams in this study are more geochemically complex than binary mixing of GW and SSW endmembers (e.g., dependent on contributions from multiple aquifers), general trends through time and in space in stream water dissolved carbon were used to provide supplemental insight and independent confirmation of mixing dynamics.

The observed shifts in stream water dissolved carbon geochemistry across subwatersheds (see Figure 8, from high DOC and low DIC/$SUVA_{254}$ to low DOC and high DIC/$SUVA_{254}$) evaluated together with the transition in GW endmember contributions to streamflow (from low to high f_{GW}) through time support our classification of the SSW endmember as a shallow, short residence time source relative to the GW endmembers. Streamflow DOC concentrations generally decreased and DIC concentrations increased as f_{GW} increased in all subwatersheds through time. The observed decreases in DOC concentrations in individual streams occurred at the same time as increases in f_{GW}, which is consistent with (1) measured GW endmember DOC concentrations, which were low and highly uniform across all well samples (38 ± 6 μM), and (2) previous work showing significant differences in dissolved organic matter (DOM) content in soil versus GW reservoirs from abiotic (e.g., sorption) and biotic (e.g., remineralization) processing (Chapelle et al., 2016; Shen et al., 2015).

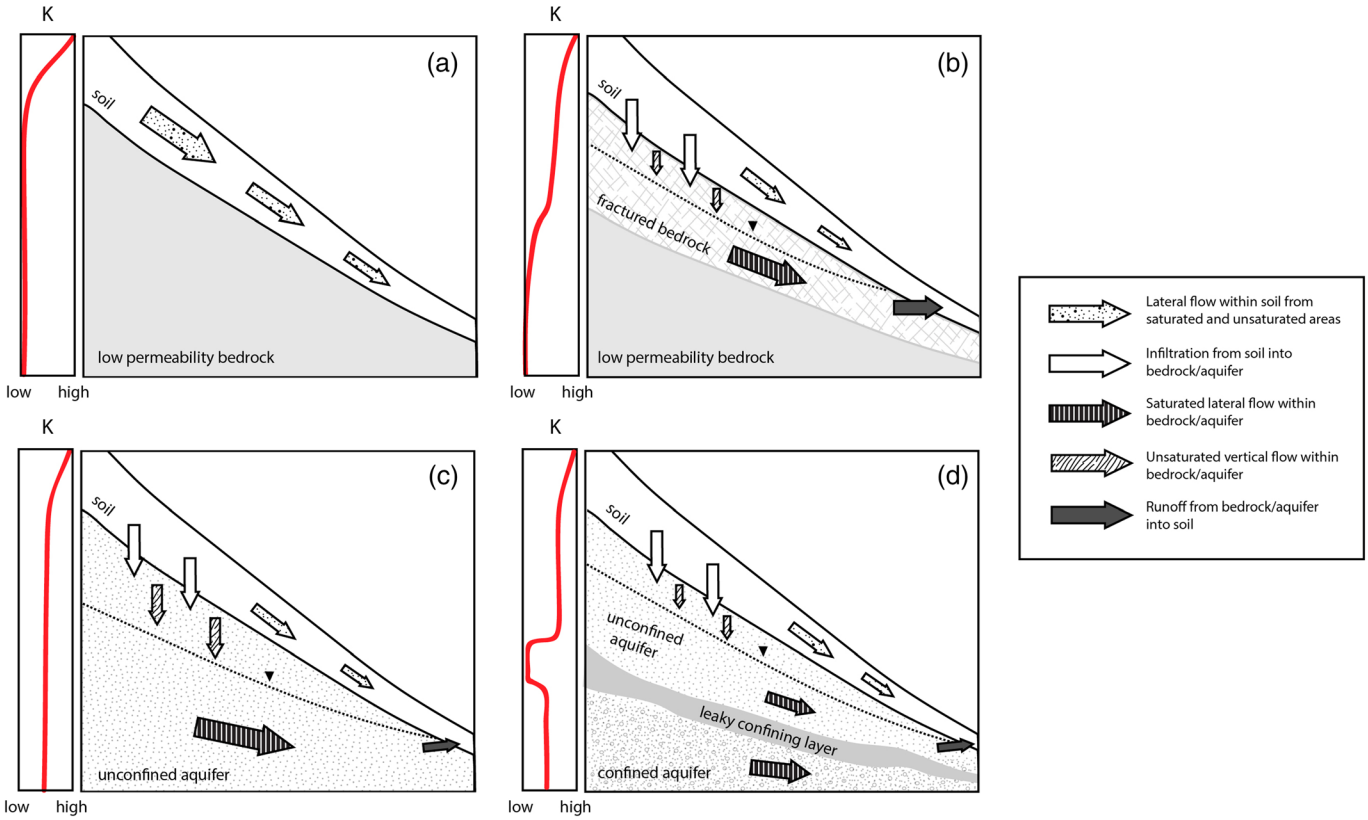

Figure 9. Conceptual diagram of baseflow generation processes in a range of geologic settings showing how various flow paths can contribute to baseflow. Each subfigure shows hillslope depictions of baseflow dominated by (a) shallow subsurface water contributions, (b) bedrock groundwater emerging as shallow subsurface water contributions, (c) groundwater contributions, and (d) groundwater contributions from multiple aquifers. All lateral arrows represent flow paths that can eventually contribute to runoff. Sideplots accompanying each subfigure show possible changes in hydraulic conductivity, K (as an indicator of permeability), with depth. Figure is not to scale and is modified from Katsura et al. (2008).

DOM quantity and quality shift during transport through the subsurface; in soils, bioavailability of DOM is typically reduced with increasing depth as microbes preferentially remineralize labile organic matter and leave behind more refractory DOM (Shen et al., 2015). Subsequent recharge of water containing this highly recycled soil DOM often leads to substantial differences in DOM concentration, composition, and bioavailability between soil water and GW (Chapelle et al., 2016; Shen et al., 2015). The high $SUVA_{254}$ values associated with higher f_{GW} in this study are consistent with an expected decrease in DOM reactivity with greater source contributions from GW. All well samples from the SLW had high $SUVA_{254}$ values (4.0 ± 1.8 L mg^{-1} m^{-1}), indicative of recycled (e.g., refractory) DOM. Initial DOC concentrations in streams were also spatially variable, which suggested that SSW endmember DOC geochemistry was distinct across subwatersheds as GW DOC concentrations were highly uniform. The uniformity in GW endmember DOC concentrations, which is common to many GW systems (Chapelle et al., 2016), allowed us to establish conservative mixing lines for approximation of SSW endmember DOC concentrations using individual projections through the stream water and GW endmember DOC data. SSW endmember DOC concentrations in western streams projected out to a lower DOC concentration SSW endmember than their eastern counterparts (Figure 10a). The lower SOM content in western subwatersheds relative to eastern subwatersheds can explain the spatial distinction in estimated SSW endmember DOC concentrations ($r_s = 0.79$), while allowing SSW DIC concentrations to remain relatively uniform otherwise (Figure 10b). The mixing lines also highlight that the rate of change in DOC concentrations with respect to f_{GW} shifts with time; changes in slope indicate a shift in process or behavior that may be best explained as intrasource variability in SSW endmember DOC concentrations, not only in space but also with time. The extrapolated decreases in SSW endmember DOC concentrations with time in subwatersheds are consistent with drainage of water in shallow

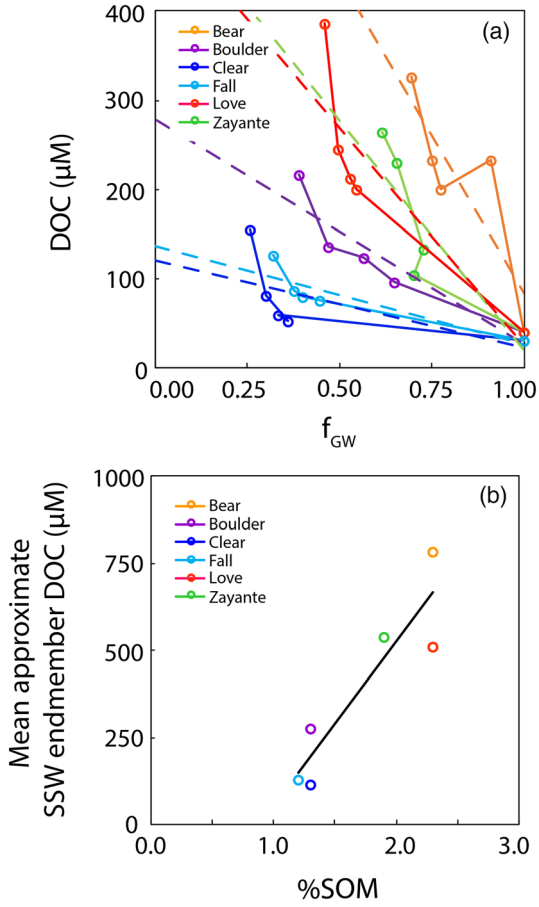

Figure 10. (a) Stream water DOC concentration versus the fraction of stream water baseflow from GW (f_{GW}) with mixing lines displayed for each stream using GW endmember DOC and stream DOC concentrations and (b) percent soil organic matter (%SOM) in each subwatershed versus the back-calculated SSW endmember DOC concentration for each subwatershed ($r_s = 0.79$).

water storage zones (whether that water is primarily transported via downslope drainage and/or as exfiltrating bedrock GW that enters the shallow zone before final discharge into proximal streams). Work by Bishop et al. (2004) showed that DOC geochemistry can be depth dependent in soils, and SOM data extracted from SSURGO confirmed this depth dependency in SOM content in SLW soils (Table S6).

Conceptually, this change in SSW endmember DOC geochemistry with time and in space can be contrasted with endmember mixing dynamics controlling stream water DIC concentrations. Slopes of regressions between f_{GW} and stream water DIC concentrations were generally consistent with time, though mixing lines were not established as GW endmember DIC concentrations were not uniform, and DIC concentrations in streams are affected by gas evasion, which can lower DIC concentrations considerably (Doctor et al., 2008; Öquist et al., 2009). Both factors would have a significant effect on mixing line projections. Nonetheless, a visual examination of stream water DIC concentrations indicates that (1) most data fall on lines with y intercepts (e.g., theoretical SSW endmember DIC concentrations) that are reasonable (e.g., positive and low DIC concentration consistent with SSW from other forested watersheds) and (2) GW endmember DIC concentrations within the range of DIC concentrations observed for GW in the area (aside from Love Creek) (Kindler et al., 2011). These general consistencies in regression behavior in DIC concentrations imply a relative stasis in both GW and SSW endmember DIC contributions through the dry down period.

Taken together, we suspect that shallow subsurface flow paths contributing to baseflow in individual subwatersheds shift spatially during the dry season as shown for other systems (Nippgen et al., 2015; Uchida et al., 2006) and that this spatial evolution of contributing areas differentially affects dissolved carbon geochemistry (Laudon et al., 2011; Zimmer & McGlynn, 2018). As sources shift, DIC concentrations change relatively uniformly in space and time, acting very broadly as a qualitative indicator of watershed-scale source transitions in this system at low flows

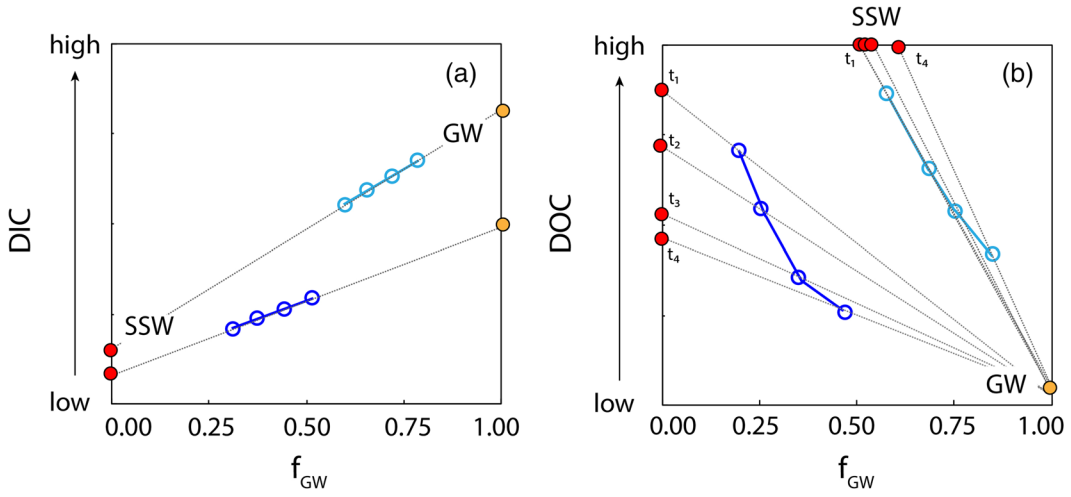

Figure 11. Generalization of hypothetical stream water dissolved carbon mixing dynamics controlled by (a) SSW and GW endmembers with relatively uniform DIC geochemistry through the summer dry down period and (b) a spatially variable SSW endmember with shifting DOC geochemistry and static GW DOC concentrations through the summer dry down period.

(e.g., low to high as a proxy for SSW to GW dominance) (Figure 11a). In contrast, DOC concentrations are indicators of subwatershed-scale SSW intrasource endmember variability as SSW storage is depleted through the seasonal baseflow recession (Figure 11b).

5. Conclusions

Source contributions to baseflow in a structurally complex central coastal California watershed were quantified using EMMA during the summer dry down period and related to spatial indices at the subwatershed scale to gain insight into the drivers of baseflow generation. Relative contributions of GW and SSW to baseflow were spatially and temporally variable across subwatersheds. While some streams transitioned to GW dominance, several streams remained dominated by SSW contributions through the baseflow recession period. Watershed controls on GW versus SSW-dominated streams appeared to arise from subwatershed-scale differences in lithology, which dictates where water can be stored and transported in the subsurface. This, in turn, influences the residence time of flow paths and the timing of streamflow contributions. At the subwatershed scale, dissolved carbon geochemistry was consistent with shifting source waters, even as contributing areas associated with each source within subwatersheds likely changed through time. Stream water DIC concentrations were broad, qualitative indicators of watershed-level transitions in dominant source waters, while DOC concentrations and $SUVA_{254}$ values were assumed to better reflect intrasource changes consistent with expected shifts in organic matter content as soil layers at different depths drained. Our findings show that using a multitracer approach for identification of source contributions to baseflow in structurally diverse watersheds can provide new insight into baseflow dynamics. These results have broad implications for our understanding of baseflow generation, and more work is needed to better understand when and where assumptions of stationarity in baseflow sources may be inappropriate.

Data Availability Statement

Data used in this study are available from the HydroShare data repository (https://www.hydroshare.org/resource/8b054e66289743f7b930358907e48f8e/).

Acknowledgments

The authors thank Nate Gillespie at the San Lorenzo Valley Water District and Ross Albert at the Scotts Valley Water District for providing historical water-quality data and access to monitoring wells for sampling and Rob Franks, Kaylee Glenney, and Carolyn Brady for field and lab assistance. We thank Andrew Fisher for providing material support. We thank Jason Parke and Barry Hecht at Balance Hydrologics and John Ricker at the County of Santa Cruz, Environmental Health Department, for useful discussions. We thank the associate editor and editor as well as three anonymous reviewers for valuable feedback that significantly improved the quality of this manuscript. This research was supported by the Geological Society of America (GSA) through two student research grants with additional support from the National Science Foundation Graduate Research Fellowship Program (DGE-1329626).

References

Anderson, M. G., & Burt, T. P. (1980). Interpretation of recession flow. *Journal of Hydrology*, *46*(1–2), 89–101. https://doi.org/10.1016/0022-1694(80)90037-2

Asano, Y., Uchida, T., Mimasu, Y., & Ohte, N. (2009). Spatial patterns of stream solute concentrations in a steep mountainous catchment with a homogeneous landscape. *Water Resources Research*, *45*, W10432. https://doi.org/10.1029/2008wr007466

Bergstrom, A., Jencso, K., & McGlynn, B. (2016). Spatiotemporal processes that contribute to hydrologic exchange between hillslopes, valley bottoms, and streams. *Water Resources Research*, *52*, 4628–4645. https://doi.org/10.1002/2015WR017972

Bishop, K., Seibert, J., Koher, S., & Laudon, H. (2004). Resolving the double paradox of rapidly mobilized old water with highly variable responses in runoff chemistry. *Hydrological Processes*, *18*(1), 185–189. https://doi.org/10.1002/hyp.5209

Bloomfield, J. P., Allen, D. J., & Griffiths, K. J. (2009). Examining geological controls on baseflow index (BFI) using regression analysis: An illustration from the Thames Basin, UK. *Journal of Hydrology*, *373*(1–2), 164–176. https://doi.org/10.1016/j.jhydrol.2009.04.025

Blumstock, M., Tetzlaff, D., Malcolm, I., Nuetzmann, G., & Soulsby, C. (2015). Baseflow dynamics: Multi-tracer surveys to assess variable groundwater contributions to montane streams under low flows. *Journal of Hydrology*, *527*, 1021–1033. https://doi.org/10.1016/j.jhydrol.2015.05.019

Brabb, E. E., Wentworth, C., Knifong, D., Graymer, R., & Blissenbach, J. (1997). *Geologic map of Santa Cruz County, California*. USGS Publications Warehouse.

Buttle, J. M., Dillon, P. J., & Eerkes, G. R. (2004). Hydrologic coupling of slopes, riparian zones and streams: An example from the Canadian Shield. *Journal of Hydrology*, *287*(1–4), 161–177. https://doi.org/10.1016/j.jhydrol.2003.09.022

Carlier, C., Wirth, S. B., Cochand, F., Hunkeler, D., & Brunner, P. (2018). Geology controls streamflow dynamics. *Journal of Hydrology*, *566*, 756–769. https://doi.org/10.1016/j.jhydrol.2018.08.069

CCAMP (2019). Central Coastal Ambient Monitoring Program, Environmental Protection Agency. Available online at www.ceden.org. Accessed January 2019., edited.

Chapelle, F. H., Shen, Y., Strom, E. W., & Benner, R. (2016). The removal kinetics of dissolved organic matter and the optical clarity of groundwater. *Hydrogeology Journal*, *24*(6), 1413–1422. https://doi.org/10.1007/s10040-016-1406-y

Christophersen, N., & Hooper, R. P. (1992). Multivariate-analysis of stream water chemical-data—The use of principal components-analysis for the end-member analysis mixing problem. *Water Resources Research*, *28*(1), 99–107. https://doi.org/10.1029/91WR02518

Christophersen, N., Neal, C., Hooper, R. P., Vogt, R. D., & Andersen, S. (1990). Modelling streamwater chemistry as a mixture of soilwater end-members—A step towards second-generation acidification models. *Journal of Hydrology*, *116*(1–4), 307–320. https://doi.org/10.1016/0022-1694(90)90130-p

Costelloe, J., Peterson, T., Halbert, K., Western, A., & McDonnell, J. (2015). Groundwater surface mapping informs sources of catchment baseflow. *Journal of Hydrology and Earth System Sciences*, *19*(4), 1599–1613. https://doi.org/10.5194/hess-19-1599-2015

Devito, K., Creed, I., Gan, T., Mendoza, C., Petrone, R., Silins, U., & Smerdon, B. (2005). A framework for broad-scale classification of hydrologic response units on the boreal plain: Is topography the last thing to consider? *Hydrological Processes*, *19*(8), 1705–1714. https://doi.org/10.1002/hyp.5881

Doctor, D. H., Kendall, C., Sebestyen, S. D., Shanley, J. B., Ohte, N., & Boyer, E. W. (2008). Carbon isotope fractionation of dissolved inorganic carbon (DIC) due to outgassing of carbon dioxide from a headwater stream. *Hydrological Processes*, *22*(14), 2410–2423. https://doi.org/10.1002/hyp.6833

Emanuel, R. E., Epstein, H. E., McGlynn, B. L., Welsch, D. L., Muth, D. J., & D'Odorico, P. (2010). Spatial and temporal controls on watershed ecohydrology in the northern Rocky Mountains. *Water Resources Research*, *46*, W11553. https://doi.org/10.1029/2009WR008890

ETIC Engineering, I. (2006). Groundwater modeling study of the Santa Margarita Groundwater Basin. A report prepared for Scotts Valley Water District., edited.

Fisher, A., Lozano, S., Beganskas, S., Teo, E., Young, K., Weir, W., Harmon, R. (2016). Regional managed aquifer recharge and runoff analyses in Santa Cruz and northern Monterey Counties, California. A report prepared for the California State Coastal Conservancy, Project 13–118, edited.

Freeze, R., & Cherry, J. A. (1979). *Groundwater*. Englewood Cliffs: Prentice-Hall Inc.

Grossmann, J., & Kloss, R. (1994). Variability of water quality in a spruce stand. *Plant Nutrition and Soil Science*, *157*(1), 47–51. https://doi.org/10.1002/jpln.19941570109

Hale, V. C., & McDonnell, J. J. (2016). Effect of bedrock permeability on stream base flow mean transit time scaling relations: 1. A multiscale catchment intercomparison. *Water Resources Research*, *52*, 1358–1374. https://doi.org/10.1002/2014WR016124

Hale, V. C., McDonnell, J. J., Stewart, M. K., Solomon, D. K., Doolitte, J., Ice, G. G., & Pack, R. T. (2016). Effect of bedrock permeability on stream base flow mean transit time scaling relationships: 2. Process study of storage and release. *Water Resources Research*, *52*, 1375–1397. https://doi.org/10.1002/2015WR017660

Harr, R. (1977). Water flux in soil and subsoil on a steep forested slope. *Journal of Hydrology*, *33*(1-2), 37–58. https://doi.org/10.1016/0022-1694(77)90097-X

Hewlett, J. D., & Hibbert, A. R. (1963). Moisture and energy conditions within a sloping soil mass during drainage. *Journal of Geophysical Research*, *68*(4), 1081–1087. https://doi.org/10.1029/JZ068i004p01081

Hooper, R. P. (2003). Diagnostic tools for mixing models of stream water chemistry. *Water Resources Research*, *39*(3), 1055. https://doi.org/10.1029/2002WR001528

Hooper, R. P., Christophersen, N., & Peters, N. E. (1990). Modeling streamwater chemistry as a mixture of soilwater end-members—An application to the Panola Mountain catchment, Georgia, USA. *Journal of Hydrology*, *116*(1–4), 321–343. https://doi.org/10.1016/0022-1694(90)90131-g

Jencso, K. G., & McGlynn, B. L. (2011). Hierarchical controls on runoff generation: Topographically driven hydrologic connectivity, geology, and vegetation. *Water Resources Research*, *47*, W11527. https://doi.org/10.1029/2011WR010666

Katsura, S., Kosugi, K., Mizutani, T., Okunaka, S., & Mizuyama, T. (2008). Effects of bedrock groundwater on spatial and temporal variations in soil mantle groundwater in a steep granitic headwater catchment. *Water Resources Research*, *44*, W09430. https://doi.org/10.1029/2007WR006610

Kennedy/Jenks (2015). Santa Margarita Basin groundwater modeling technical study. A report prepared for Scotts Valley Water District.

Kindler, R., Siemens, J., Kaiser, K., Walmsley, D. C., Bernhofer, C., Buchmann, N., et al. (2011). Dissolved carbon leaching from soil is a crucial component of the net ecosystem carbon balance. *Global Change Biology*, *17*(2), 1167–1185. https://doi.org/10.1111/j.1365-2486.2010.02282.x

Klaus, J., & McDonnell, J. J. (2013). Hydrograph separation using stable isotopes: Review and evaluation. *Journal of Hydrology*, *505*, 47–64. https://doi.org/10.1016/j.jhydrol.2013.09.006

Laudon, H., Berggren, M., Agren, A., Buffam, I., Bishop, K., Grabs, T., et al. (2011). Patterns and dynamics of dissolved organic carbon (DOC) in boreal streams: The role of processes, connectivity, and scaling. *Ecosystems*, *14*(6), 880–893. https://doi.org/10.1007/s10021-011-9452-8

Manderscheid, B., & Matzner, E. (1995). Spatial and temporal variation of soil solution chemistry and ion fluxes through the soil in a mature Norway spruce (*Picea abies* (L.) Karst.) stand. *Biogeochemistry*, *30*(2), 99–114. https://doi.org/10.1007/BF00002726

McCallum, J. L., Cook, P. G., Brunner, P., & Berhane, D. (2010). Solute dynamics during bank storage flows and implications for chemical base flow separation. *Water Resources Research*, *46*, W07541. https://doi.org/10.1029/2009WR008539

McDonnell, J. J., & Woods, R. (2004). On the need for catchment classification. *Journal of Hydrology*, *299*(1-2), 2–3. https://doi.org/10.1016/j.jhydrol.2004.09.003

McGuire, K. J., McDonnell, J. J., Weiler, M., Kendall, C., McGlynn, B. L., Welker, J. M., & Seibert, J. (2005). The role of topography on catchment-scale water residence time. *Water Resources Research*, *41*, W05002. https://doi.org/10.1029/2004WR003657

Mosley, M. P. (1979). Streamflow generation in a forested watershed, New Zealand. *Water Resources Research*, *15*(4), 795–806. https://doi.org/10.1029/WR015i004p00795

NCDC (2019). National Centers for Environmental Information Climate Data Online. Available online at https://www.ncdc.noaa.gov/

Nippgen, F., McGlynn, B. L., & Emanuel, R. E. (2015). The spatial and temporal evolution of contributing areas. *Water Resources Research*, *51*, 4550–4573. https://doi.org/10.1002/2014WR016719

Nippgen, F., McGlynn, B. L., Emanuel, R. E., & Vose, J. M. (2016). Watershed memory at the Coweeta Hydrologic Laboratory: The effect of past precipitation and storage on hydrologic response. *Water Resources Research*, *52*, 1673–1695. https://doi.org/10.1002/2015WR018196

NLCD (2011). National Land Cover Database, Multi-Resolution Land Characteristics Consortium. Available online at https://www.mrlc.gov/data

NTN (2019). *National Trends Network, National Atmospheric Deposition Program*. Madison, WI: NADP Program Office, Wisconsin State Laboratory of Hygiene. Available online at http://nadp.slh.wisc.edu/

Onda, Y., Tsujimura, M., Fujihara, J. I., & Ito, J. (2006). Runoff generation mechanisms in high-relief mountainous watersheds with different underlying geology. *Journal of Hydrology*, *331*(3–4), 659–673. https://doi.org/10.1016/j.jhydrol.2006.06.009

Öquist, M. G., Wallin, M., Seibert, J., Bishop, K., & Laudon, H. (2009). Dissolved inorganic carbon export across the soil/stream interface and its fate in a boreal headwater stream. *Environmental Science and Technology*, *43*(19), 7364–7369. https://doi.org/10.1021/es900416h

Payn, R. A., Gooseff, M. N., McGlynn, B. L., Bencala, K. E., & Wondzell, S. M. (2012). Exploring changes in the spatial distribution of stream baseflow generation during a seasonal recession. *Water Resources Research*, *48*, W04519. https://doi.org/10.1029/2011WR011552

Pfister, L., Martinez-Carreras, N., Hissler, C., Klaus, J., Carrer, G. E., Stewart, M. K., & McDonnell, J. J. (2017). Bedrock geology controls on catchment storage, mixing, and release: A comparative analysis of 16 nested catchments. *Hydrological Processes*, *31*(10), 1828–1845. https://doi.org/10.1002/hyp.11134

Price, K. (2011). Effects of watershed topography, soils, land use, and climate on baseflow hydrology in humid regions: A review. *Progress in Physical Geography*, *35*(4), 465–492. https://doi.org/10.1177/0309133311402714

Rantz, S. E. (1982). *Measurement and computation of streamflow*. Washington, DC: US Department of the Interior, USGS.

Shen, Y., Chapelle, F. H., Strom, E. W., & Benner, R. (2015). Origins and bioavailability of dissolved organic matter in groundwater. *Biogeochemistry*, *122*(1), 61–78. https://doi.org/10.1007/s10533-014-0029-4

Sivapalan, M. (2003). Process complexity at hillslope scale, process simplicity at the watershed scale: Is there a connection? *Hydrological Processes*, *17*(5), 1037–1041. https://doi.org/10.1002/hyp.5109

Smakhtin, V. U. (2001). Low flow hydrology: A review. *Journal of Hydrology*, *240*(3–4), 147–186. https://doi.org/10.1016/s0022-1694(00)00340-1

Smerdon, B. D., Gardner, W. P., Harrington, G. A., & Tickell, S. J. (2012). Identifying the contribution of regional groundwater to the baseflow of a tropical river (Daly River, Australia). *Journal of Hydrology*, *464-465*, 107–115. https://doi.org/10.1016/j.jhydrol.2012.06.058

Soulsby, C., Tetzlaff, D., van den Bedem, N., Malcolm, I. A., Bacon, P. J., & Youngson, A. F. (2007). Inferring groundwater influences on surface water in montane catchments from hydrochemical surveys of springs and streamwaters. *Journal of Hydrology*, *333*(2–4), 199–213. https://doi.org/10.1016/j.jhydrol.2006.08.016

SSURGO (2019). Soil Survey Staff, Natural Resources Conservation Service, United States Department of Agriculture. Web Soil Survey. Available online at https://websoilsurvey.nrcs.usda.gov/

Stoelzle, M., Schuetz, T., Weiler, M., Stahl, K., & Tallaksen, L. M. (2019). Beyond binary baseflow separation: Delayed flow index as a fresh perspective on streamflow contributions. *Journal of Hydrology and Earth System Sciences Discussions*, 1–30. https://doi.org/10.5194/hess-24-849-2020

Tague, C., & Grant, G. E. (2004). A geological framework for interpreting the low-flow regimes of Cascade streams, Willamette River Basin, Oregon. *Water Resources Research*, *40*, W04303. https://doi.org/10.1029/2003WR002629

Tallaksen, L. (1995). A review of baseflow recession analysis. *Journal of Hydrology*, *165*(1–4), 349–370. https://doi.org/10.1016/0022-1694(94)02540-R

Temnerud, J., Folster, J., Buffam, I., Laudon, H., Erlandsson, M., & Bishop, K. (2010). Can the distribution of headwater stream chemistry be predicted from downstream observations? *Hydrological Processes*, *24*(16), 2269–2276. https://doi.org/10.1002/hyp.7615

Tetzlaff, D., & Soulsby, C. (2008). Sources of baseflow in larger catchments—Using tracers to develop a holistic understanding of runoff generation. *Journal of Hydrology*, *359*(3–4), 287–302. https://doi.org/10.1016/j.jhydrol.2008.07.008

Uchida, T., Asano, Y., Ohte, N., & Mizuyama, T. (2003). Seepage area and rate of bedrock groundwater discharge at a granitic unchanneled hillslope. *Water Resources Research*, *39*(1), 1018. https://doi.org/10.1029/2002WR001298

Uchida, T., McDonnell, J. J., & Asano, Y. (2006). Functional intercomparison of hillslopes and small catchments by examining water source, flowpath and mean residence time. *Journal of Hydrology*, *327*(3–4), 627–642. https://doi.org/10.1016/j.jhydrol.2006.02.037

Wagener, T., Sivapalan, M., Troch, P., & Woods, R. (2007). Catchment classification and hydrologic similarity. *Geography Compass*, *1*(4), 901–931. https://doi.org/10.1111/j.1749-8198.2007.00039.x

Weishaar, J. L., Aiken, G. R., Bergamaschi, B. A., Fram, M. S., Fujii, R., & Mopper, K. (2003). Evaluation of specific ultraviolet absorbance as an indicator of the chemical composition and reactivity of dissolved organic carbon. *Environmental Science and Technology*, *37*(20), 4702–4708. https://doi.org/10.1021/es030360x

Zimmer, M. A., Bailey, S. W., McGuire, K. J., & Bullen, T. D. (2013). Fine scale variations of surface water chemistry in an ephemeral to perennial drainage network. *Hydrological Processes*, *27*(24), 3438–3451. https://doi.org/10.1002/hyp.9449

Zimmer, M. A., & Gannon, J. P. (2018). Run-off processes from mountains to foothills: The role of soil stratigraphy and structure in influencing run-off characteristics across high to low relief landscapes. *Hydrological Processes*, *32*(11), 1546–1560. https://doi.org/10.1002/hyp.11488

Zimmer, M. A., & McGlynn, B. L. (2018). Lateral, vertical, and longitudinal source area connectivity drive runoff and carbon export across watershed scales. *Water Resources Research*, *54*, 1576–1598. https://doi.org/10.1002/2017WR021718